Kinetic Barriers of H-Atom Transfer Reactions in Alkyl, Allylic, and Oxoallylic Radicals as Calculated by Composite Ab Initio Methods

Carrigan J. Hayes and Donald R. Burgess, Jr.*

National Institute of Standards and Technology; 100 Bureau Drive, Stop 8320, Gaithersburg, Maryland 20899-8320

Received: November 18, 2008; Revised Manuscript Received: January 15, 2009

Composite ab initio and density functional theory (DFT) methods were used to explore internal hydrogen-atom transfers in a variety of primary, secondary, and tertiary alkyl and functionalized radicals with implications for combustion environments. The composite ab initio method G3MP2B3 was found to achieve the most reasonable balance between accuracy and economy in modeling the energetics of these reactions. Increased alkyl substitution reduced barriers to isomerization by about 10 and 20 kJ mol^{-1} for secondary and tertiary radical formation, respectively, relative to primary radical reactions and was relatively insensitive to the transition-state ring size (extent of H-atom internal shift). Reactions involving alkenyl and alkanoyl radicals were also explored. Hydrogen-atom transfers involving allylic radical formation demonstrated barrier heights that were 15−20 kJ mol^{-1} lower than those in corresponding alkyl radicals, whereas those involving oxoallylic species (α-site radicals of aldehydes and ketones) were 20−40 kJ mol^{-1} lower. In the cases of the alkyl radicals, enthalpies of activation were seen to scale with enthalpies of reaction. This correlation was not seen, however, in the cases of the allylic and oxoallylic radicals; this fact has significant implications in combustion chemistry and mechanism development, considering that such Evans−Polanyi correlations are widely used in estimating barrier heights for rate expressions.

Introduction

America's rapidly changing energy requirements necessitate efforts to understand new types of fuels and new combustion technologies. Kinetic modeling provides an enormously useful tool for predicting the chemistry of new fuels and combustion environments; however, kinetic mechanisms (also termed models) for this chemistry must first be developed. Crucial thermochemical and chemical kinetic data can be generated via experiment, theory, and estimation methods. Chemical mechanism development involves substantial collaborative effort among different research groups employing different measurement and computational techniques; this need for complementary efforts becomes increasingly evident as the complexities of the fuels of interest increase. In particular, NIST's (National Institute of Standards and Technology) Real Fuels Project[1] seeks to address the challenges of mechanism development via a three-pronged approach: first, by experimentally monitoring the kinetics of hydrocarbon combustion (alkyl radical and alkylperoxy radical chemistry);[2−7] second, by computationally generating thermochemical and chemical kinetic data for relevant species and reactions; and third, by maintaining databases[8−11] wherein this information can be readily shared. This article reports on recent efforts toward the second of these objectives.

Reactions used in combustion mechanisms are generally subdivided into classes to make their treatment more tractable; common classes include bond fissions, β scissions, molecular eliminations, abstractions, and isomerizations. One type of isomerization involves hydrogen-atom transfers that convert one alkyl radical to another. Such isomerizations play key roles in the combustion of most fuels and fuel additives, from small alkanes to aromatic hydrocarbons as well as to functionalized species (such as alkyl esters) with potential implications for alternative fuel chemistry (i.e., biodiesel). These H-atom transfers, sometimes termed "migrations," are fundamentally internal abstraction reactions.

There have been various methodologies reported in the literature for estimating kinetic parameters for classes of reactions. These methodologies generally employ group additivity[12] schemes based on structure activity relationships (SARs). These methods heavily rely on the Evans−Polanyi principle, which is an observation that there is often a linear correlation between activation energies (E_a) and reaction enthalpies (ΔH_{rxn}) within a series of closely related reactions.[13] In this article, we specifically discuss two instances that employ this principle and refer the reader to other studies[14−16] for information on the use of reaction classes in developing chemical kinetic models for combustion applications.

In one systematic study, Curran et al.[17] classified reactions pertaining to alkane combustion as belonging to one of several reaction types, one of which was alkyl radical isomerization. In treating H-atom transfers, they considered the strength of the C−H bond being broken and the ring strain energy present in the transition state to generate the overall activation energy, E_a (eq 1), where ΔH_{rxn} reflects the enthalpy of the endothermic reaction, E_{strain} is the ring strain computed using group additivity,[12] and E_{abstr} is the nascent barrier to abstraction computed using eq 2

$$E_a = \Delta H_{rxn} + E_{strain} + E_{abstr} \quad (1)$$

$$E_{abstr} = 53.1 + (0.37\Delta H_{rxn})\ \text{kJ mol}^{-1} \quad (2)$$

Similarly, Matheu et al.[18] determined Arrhenius rate parameters for reactions using a similar formalism, as expressed in eq 3. The parameters a and b in eq 3 were generated from a least-squares fit of activation energies derived from density

* Corresponding author. E-mail: dburgess@nist.gov. Fax: 301-869-4020.

10.1021/jp810147z
Published on Web 02/18/2009

functional theory (DFT) calculations, which provided an Evans−Polanyi rule, where ΔH_{rxn} refers to the enthalpies of reaction estimated using the GAPP (group additivity property predictor)[19] model and E_{strain} refers to the ring-strain energy

$$E_{abstr} = a + b\Delta H_{rxn} + E_{strain} \quad (3)$$

The methods employed by Curran et al.[17] and by Matheu et al.[18] have both achieved much success in various applications and utilize both empirical treatments and a variety of computational methods in approximating the kinetics of given elementary reaction steps as a function of their thermodynamic properties.

Although they generally perform well, composite ab initio methods have not been used as extensively in predictive methods to look at discrete reaction steps because of significant computational costs. However, these methods have recently become more affordable because of increases in computer processor speeds, primary memory, and scratch disk space. These improvements have enabled a thorough and accurate examination of trends in barrier heights seen in isomerization reactions involving alkyl radicals and functionalized derivatives.

Previously, we demonstrated[20] that the modified composite ab initio method G3MP2B3 performs well in replicating the energies predicted by various other composite methods including G3B3 and CBS-QB3 (which themselves are considered to be quantitatively comparable to experimental results) at far less computational cost. Therefore, an exhaustive computational assessment of the 1,2- through 1,7-H-atom transfers in a variety of chemical environments is a tractable goal; in the present study, these isomerizations have been examined for alkyl radicals as well as radicals of alkenes (alkenyl and allylic radicals) and aldehydes (alkanoyl and oxoallylic radicals). (In allylic and oxoallylic radicals, the radical sites are immediately adjacent (α) to an unsaturated carbon, for example, CH_3—CH*—CH═CH_2 (but-1-en-3-yl) and CH_3—CH*—CH(═O) (prop-2-anoyl).) The classes of alkenyl and alkanoyl radicals are more general and refer to any radical containing both a double bond and radical center or carbonyl group and radical center, respectively.) This study will allow us to explore details of isomerization barrier heights in different classes of molecules systematically and thoroughly.

Other research groups have used experimental or computational techniques to explore details of isomerizations and related reactions in alkyl radical and alkylperoxy radical chemistry. We mention just a few of these here. Pilling and coworkers[21] have studied hydrogen-atom transfers and other reactions involving the pentyl radical system using quantum chemical methods and master equation modeling. Taatjes and coworkers[22] have combined measured time-dependent product profiles with quantum calculations, master equation modeling, and chemical kinetics modeling to investigate the kinetics of the reaction of O_2 with the cyclohexyl radical, paying particular attention to isomerization reactions and peroxy radical chemistry, including ring opening and closing reactions. Koshi and coworkers[23] have used quantum chemical methods to determine rates of alkoxy−alkylperoxy radical reactions including H-atom transfers and cyclic ether formation reactions. A number of workers have utilized quantum chemical methods to investigate isomerization reactions involving alkylperoxy radicals including the work by Merle et al.,[24] DeSain et al.,[25] and Chan et al.[26] Of great interest recently, because of the emerging potential of biodiesel fuels, are recent computational investigations by Pitz and coworkers,[27] Violi and coworkers,[28] and Simmie and coworkers[29] of reaction pathways relevant to the combustion of methyl esters.

Computational Methods. The composite ab initio methods G3MP2B3 and G3B3,[30,31] variants of Gaussian 3 (G3), were used to calculate thermochemical and chemical kinetic parameters for reactions of interest in hydrocarbon combustion. These variants use B3LYP/6-31G(d)[32,33] geometries and zero-point energies instead of the MP2/6-31G(d) geometries and HF/6-31G(d) zero-point energies used in the root G3 methods. Molecular geometries derived from B3LYP/6-31G(d) and other DFT calculations have usually been observed to perform better than ab initio geometries for use in energy calculations of radicals species. Additional calibrations were performed using CBS-QB3[34] calculations. The results were also compared with those obtained via hybrid DFT methods such as MPW1K.[35] All calculations were performed using Gaussian 03.[36] This study utilized the high-performance computational capabilities of the Biowulf Linux cluster at the National Institutes of Health, Bethesda, Maryland (http://biowulf.nih.gov).[37]

Providing rigorous quantitative uncertainties for molecular energies derived from quantum calculations is difficult. In practice, this is usually done by computing values for a set of molecules, comparing the values to well-established experimental values, and then characterizing the uncertainties in the computed values using mean average deviations. Such comparisons, of course, require data sets with well-established experimental values. In this work, where we are primarily computing the barriers to H-atom isomerizations, these values are unknown and are not directly measurable through experimental methods, although indirect measurements can be obtained through kinetic analyses of complex series of reactions, such as those obtainable through shock tube studies.[2−4] Rigorous assignment of quantitative uncertainties is not possible with quantum calculations; consequently, we must rely on estimates of uncertainties in various fashions.

There are a number of sources of uncertainties in molecular energies derived from quantum calculations, including computed zero-point energies and empirical corrections. Other issues arise in the treatment of radical species, particularly in resonance-stabilized systems, and still others in calculations involving transition states that have nonstandard elongated bonds. We have assigned the following estimated uncertainties to enthalpies of formation computed for various species on the basis of observed trends associated with increased functionalities in the molecule: atoms (0.0 kJ mol^{-1}), alkanes (2.0 kJ mol^{-1}), alkenes and alkanals (4.0 kJ mol^{-1}), alkyl radicals (6.0 kJ mol^{-1}), and allylic and oxoallylic radicals (8.0 kJ mol^{-1}). We have assigned the following estimated uncertainties to H-atom isomerization barriers computed in this work: isomerizations involving alkyl radicals (6.0 kJ mol^{-1}) and isomerizations involving allylic and oxoallylic radicals (8.0 kJ mol^{-1}).

Results and Discussion

In the following section, we first discuss and justify our computational rationale. We then present and discuss computed barriers to reaction for isomerization reactions involving H-atom transfers in hydrocarbon radicals. Whereas we calculated several thermodynamic values in exploring these reactions, the data presented here are expressed in terms of activation barriers ($\Delta H_0^{\ddagger} = \Delta E_0^{\ddagger}$) and reaction enthalpies (ΔH_{rxn}) at 0 K. (The terms "reaction barriers" and "enthalpies of activation" will also be used interchangeably with "activation barriers".)

Briefly, our findings are three-fold. First, barrier heights for 1,5- and 1,6-H-atom transfers are significantly lower than those for shorter "migrations" by 30 to 100 kJ mol^{-1} as a result of minimal strain (conformational interactions) in the cyclic-

TABLE 1: Calculated Enthalpies of Activation at 0 K for Different Computational Methods Relative to G3MPB3

	$E_0(1° \rightarrow 1°)$/kJ mol^{-1}			$E_0(2° \rightarrow 2°)$/kJ mol^{-1}			$E_0(1° \rightarrow 2°)$/kJ mol^{-1}		
transfer	ΔCB[a]	ΔMP[b]	ΔB3[c]	ΔCB	ΔMP	ΔB3	ΔCB	ΔMP	ΔB3
2	1	15	19	−1	15	18	1	23	16
3	−1	13	11	−3	15	11	−3	13	14
4	−4	8	4	−4	12	7	−5	6	1
5	−6	4	−1	−5	12	8	−6	7	1
6	−5	8	−1	−6	13	8	−6	10	0

[a] ΔCB denotes E_0(CBS-QB3) − E_0(G3MP2B3). [b] ΔMP denotes E_0(MPW1K/6-31+G(d,p)) − E_0(G3MP2B3). [c] ΔB3 denotes E_0(B3LYP/6-31G(d)) − E_0(G3MP2B3).

transition-state structures. Second, barriers for reactions involving secondary and tertiary radicals are lower by 10−20 kJ mol^{-1} than those involving primary radicals, which is consistent with the greater stability of secondary and tertiary radicals. Third, reaction barriers for transfers involving H atoms immediately adjacent (α) to unsaturated functionalities (i.e., allylic and oxoallylic C−H bonds in alkenes and aldehydes/ketones, respectively) are significantly lower than those involving simple alkane radicals by 20−40 kJ mol^{-1}, a finding that is consistent with the greater stability of the radicals and transition states due to resonance stabilization effects. We expand on these statements in the next sections.

Methodological Survey of Alkyl Radical Isomerization. We first investigated the dependence of calculated barriers on the level of theory used to compute the barriers. Previous work in our group[20] has shown that the composite ab initio method G3MP2B3 balances computational expense and accuracy; this method was selected for the bulk of our work, along with G3B3 and CBS-QB3 calculations for calibration purposes.

Throughout this work, G3MP2B3 replicated trends seen with G3B3 within about 2 kJ mol^{-1}. The CBS-QB3 method gave comparable results to the G3 methods but with systematically slightly lower barrier heights (3−6 kJ mol^{-1}). These differences appeared to be sensitive to the complete basis set extrapolation and empirical correction terms in the CBS-Q method (uncorrected differences were <2 kJ mol^{-1}), as has been observed by others.[38] Hybrid DFT calculations were also explored because of their low computational cost when compared with ab initio methods. B3LYP and MPW1K calculations were performed using the 6-31G(d) and 6-31+G(d,p) basis sets. The DFT approaches, however, obtained mixed and generally unacceptable results: whereas the DFT barriers were either low or high by a relatively consistent amount compared with the G3MP2B3 barriers for each class of reactions, this "consistent" amount varied from one reaction class to another. For example, as shown in Table 1, the computationally inexpensive B3LYP/6-31(d) method fared fortuitously well in some cases, matching the G3MP2B3 barriers within 2 kJ mol^{-1}, but poorly in other cases, missing the G3MP2B3 barrier by as much as 10−20 kJ mol^{-1}. The MPW1K method,[35] which has been optimized for transition states, consistently performed better than other DFT methods in replicating trends in the composite ab initio results. However, on the basis of these results alone, it would be difficult to assign an uncertainty of less than 10 kJ mol^{-1} for barriers computed using this method. G3MP2B3 was determined to be the best method with regard to computational costs and accuracy for this particular study.

Overview of Potential Isomerization Pathways. The nomenclature of internal H-atom transfer reactions involves a "1,*n*" designation in which *n* refers to the position of the product radical relative to the reactant radical. In addition, a shorthand is used to designate radical type: "1°" denotes a primary radical

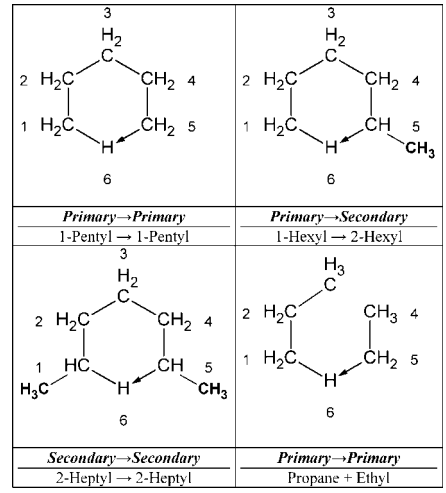

Figure 1. Six-membered cyclic transition states for 1,5-H-atom transfer reactions (internal isomerizations). Included for comparison is a simple abstraction reaction.

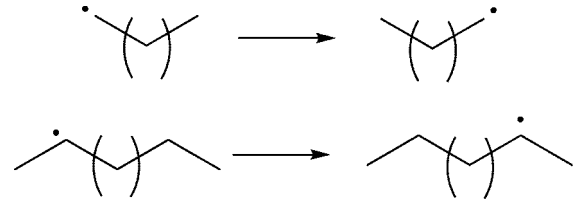

Figure 2. Primary → primary H-atom transfer reactions.

(e.g., 1-propyl), whereas "2°" denotes a secondary radical (e.g., isopropyl) and "3°" denotes a tertiary radical (e.g., *tert*-butyl).

Figure 1 shows several possible H-atom transfer isomerization reactions (internal abstractions) as well as an H-atom abstraction for comparison. The isomerization examples show 1,5-H-atom transfers with six-membered transition states. More generic illustrations of primary and secondary H-atom transfer isomerizations are given in Figure 2; other possible types of H-atom transfers involving primary, secondary, and tertiary sites are illustrated in Figure 3.

These reactions are isomerizations that are essentially internal abstraction reactions and bear similarities to bimolecular abstraction reactions such as propane + ethyl → 1-propyl + ethane (also shown in Figure 1). The main difference between the unimolecular isomerizations (internal abstraction) and the bimolecular abstraction reactions is that in an isomerization the molecule must be arranged in a rotameric conformation such that the C−H bond is accessible to the radical site. Therefore, there is a conformational energy (ring strain) that is associated with this cyclic-transition-state structure.

It should be noted that 1,2-H-atom transfers are not "internal abstractions" but are atom migrations because they involve a bridge structure in the transition state. They are pericyclic

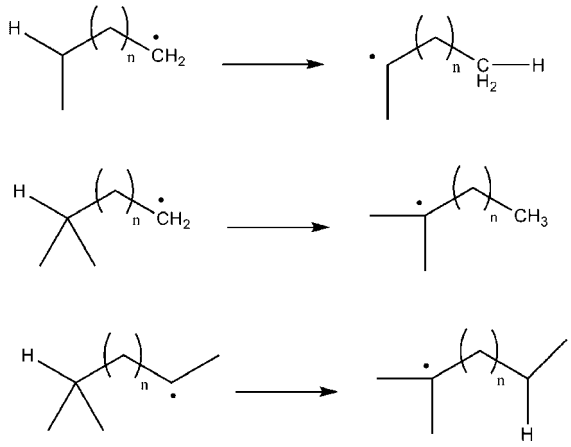

Figure 3. Other secondary (2°) and tertiary (3°) H-atom transfers: 1° → 2°, 1° → 3°, and 2° → 3°.

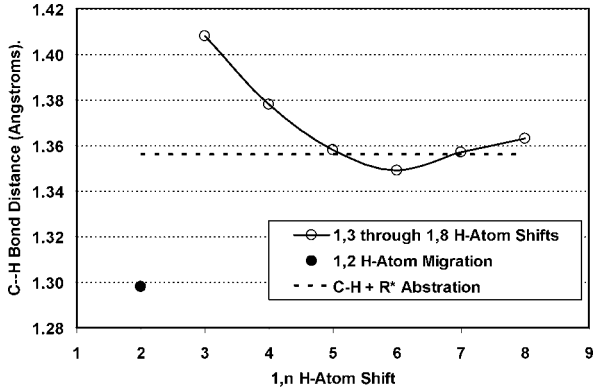

Figure 4. C−H bond distances in transition states of 1,*n* H-atom transfers and 1,2-H-atom migration compared with the C−H + R abstraction reaction.

reactions where there is a concerted rearrangement involving a π-bonded system. The different nature of this reaction type is evident in several different ways.

First, when bond lengths are considered, other 1,*n* H-atom transfers have bond lengths equivalent to those for abstraction reactions. For the primary → primary identity isomerizations in 1-propyl through 1-octyl radicals (1,3- through 1,8-H-atom transfers), the calculated [B3LYP/6-31G(d)] C−H bond lengths in the transition states are: 1.408, 1.378, 1.358, 1.349, 1.357, and 1.363 Å, respectively. That is, the C−H bond lengths for these isomerizations are about 0.00 to 0.05 Å larger than those for pure abstraction reactions (calculated to be 1.356 Å in the transition state of the reaction propane + 1-propyl). However, for ethyl isomerization (1,2-H-atom migration), the C−H bond length in the transition state is 1.298 Å or significantly smaller (0.06 to 0.11 Å) than that in larger H-atom transfers, which is consistent with a bridgelike structure. These data are presented in Figure 4, which clearly demonstrates that 1,2-H-atom migrations are a fundamentally different type of reaction than other 1,*n* H-atom transfers.

Second, the geometrical configurations in the transition states also set the 1,2-H-atom transfer apart. For both the 1,*n* H-atom transfers and the pure abstractions, the C-atom sites involved in the transition state are nonplanar, and the reaction sites are nearly tetrahedral (sp^3-like), with the hydrogen atoms not involved in the reaction coordinate nearly 30° out-of-plane. In contrast, for 1,2-H-atom migrations, the C sites are nearly planar (sp^2-like), with the nonreacting, vinylic-like C−H bonds being only 10° out-of-plane.

In the 1,*n* H-atom transfers and the pure abstractions, one C−H sigma (σ) bond is formed as another C−H σ bond is destroyed. This is also the case in the 1,2-H-atom migrations; however, given the adjacent locations of the abstracting radical and the abstracted hydrogen, this reaction also involves a degree of rehybridization (to sp^2) and C−C pi (π) bond formation. (This rehybridization is a function of the reaction coordinate, and neither reactant nor product contains a double bond. However, the transition state looks much like ethylene (sp^2) with a bridged H-atom.) This rehybridization lowers the activation energy by facilitating the transfer of the H atom between the two adjacent carbon atoms in a planar arrangement and results in the 1,2-H-atom migration barriers being lower than those in the 1,3-H-atom transfers. (The extent of these trends will be discussed subsequently.) This is the reverse of the trend predicted by considering ring strain alone. In short, the 1,*n* H-atom transfers are functionally abstraction reactions such as $CH_3CH_2-H + {}^*CH_3 \rightarrow CH_3CH_2{}^* + CH_4$ (ethane + methyl → ethyl + methane), whereas 1,2-H-atom migrations are functionally similar to metathesis reactions such as ${}^*CH_2-CH_2-H + {}^*CH_3 \rightarrow CH_2{=}CH_2 + CH_4$ (ethyl + methyl → ethene + methane), where the C−H bond being abstracted is β to a radical site.

Table 2 lists enthalpies of formation [$\Delta_f H_o$(0 K)] calculated using atomization energies obtained from the G3MP2B3 method for a representative sample of primary, secondary, and tertiary hydrocarbon radicals and for representative allylic and oxoallylic radicals. (A more expansive set is given in Supporting Information.) Additionally, relevant C−H and C−C bond dissociation energies (BDEs) have been calculated for both the parent molecules (C−H bond fissions for alkanes losing H to form alkyl radicals; e.g., butane → 1-butyl + H) and BDEs for the radicals themselves [C−H β scissions for alkyl radicals losing H to produce alkenes (e.g., 1-butyl → 1-butene + H) and C−C β scissions for alkyl radicals losing R groups to produce alkenes (e.g., 1-butyl → ethene + ethyl)]. These data show that secondary and tertiary radicals are more stable than primary radicals by 10−12 and 16−18 kJ mol^{-1}, respectively, or equivalently, that the C−H BDEs in the parent alkanes are weaker for the branched species. The data in this table also show that allylic and oxoallylic radicals are more stable than the corresponding alkyl radicals by about 50 and 30 kJ mol^{-1}, respectively.

Alkyl Radicals. Enthalpies of formation and barriers to reaction (at 0 K, via G3MP2B3) for H-atom transfer reactions involving the formation of primary radicals from primary radicals (primary → primary) are summarized in Table 3 and presented in full in the Supporting Information. This type of reaction is denoted by a "1° → 1°". In the transfer column, "2" denotes that the H-atom is transferred to two-position relative to the initial site (e.g., ethyl → ethyl), "3" denotes transfer to a relative three-position (e.g., 1-propyl → 1-propyl), and so on. (Note that in Table 3 and elsewhere in this article we always write the reactions in the exothermic direction (e.g., 1-propyl → 2-propyl) and provide barriers to reaction in this direction, which is most characteristic of the reaction. The barriers in the reverse direction (endothermic) are simply higher by an amount equal to the enthalpy of reaction.)

The primary → primary transfers summarized in Table 3 (a more detailed list is given in the Supporting Information) are mainly of theoretical importance (and will not affect kinetic pathways) because they are identity reactions in which the reactant and product are the same molecule: the H-atom has just migrated from one (identical) end of the molecule to the other. These barriers are still useful because they allow

TABLE 2: G3MP2B3 Enthalpies of Formation and Related Bond Dissociation Energies at 0 K for Representative Primary, Secondary, and Tertiary Alkyl Radicals and for Allylic and Oxoallylic Radicals[a]

formula	species	type	$\Delta_f H_0$(0 K)/kJ mol^{-1}	D_0(RC−H)/kJ mol^{-1}[b]	D_0(*RC−H)/kJ mol^{-1}[c]	D_0(*RC−C)/kJ mol^{-1}[d]
C_4H_9	1-butyl	1°	104.9	417.3	130.9	88.6
C_4H_9	*iso*-butyl	1°	97.2	417.8	122.1	88.0
C_4H_9	2-butyl	2°	93.3	405.7	142.4	91.4
C_5H_{11}	*tert*-pentyl	3°	67.9	401.4	139.6	86.7
C_5H_9	pent-1-en-5-yl	1°	202.3	414.1		
C_5H_9	pent-1-en-4-yl	2°	193.3	405.2		
C_5H_9	pent-1-en-3-yl	allylic	139.9	351.7		
$C_4H_7O_1$	but-4-anoyl	1°	15.9	417.7		
$C_4H_7O_1$	but-3-anoyl	2°	4.2	406.0		
$C_4H_7O_1$	but-2-anoyl	oxoallylic	−28.0	373.9		

[a] See the Supporting Information for additional data. [b] C−H bond fission from alkanes: C−H → CC* + H. [c] C−H β scission to alkenes: *CC−H → C=C + H. [d] C−C β scission to alkenes: *CC−C → C=C + C.

TABLE 3: G3MP2B3 Enthalpies of Activation at 0 K for H-Atom Transfers Involving Alkyl Radicals[a]

transfer	E_0(1° → 1°)/kJ mol^{-1}	E_0(2° → 2°)/kJ mol^{-1}	E_0(1° → 2°)/kJ mol^{-1}	E_0(2° → 3°)/kJ mol^{-1}	E_0(1° → 3°)/kJ mol^{-1}
2	168.3	165.5	159.5	163.5	151.9
3	169.3	167.9	162.4	161.1	156.8
4	105.6	99.8	98.3	91.0	88.6
5	78.4	73.1	68.4	62.9	60.7
6	75.9	67.9	66.1	58.3	58.9
7	91.8	85.0	82.7	68.2	68.2
$\Delta(E_a)^b$	+9	+2	0	−7	−9

[a] See the Supporting Information for data for individual reactions. [b] Average barriers for unstrained structures relative to primary → secondary radical isomerizations (1° → 2°) in alkyl radicals.

observation of trends in the dependence of barriers to H-atom migration on the type of radical sites (e.g., primary versus secondary) that are involved. Furthermore, nonidentity primary → primary transfers are possible in highly branched species, such as radicals of isoalkanes [CC(C)CC* → *CC(C)CC (3-methylbut-1-yl → 3-methylbut-4-yl)] or radicals of neoalkanes [CC(C)$_2$CC* → *CC(C)$_2$CC (3,3-dimethylbut-1-yl → 3,3-dimethylbut-4-yl)].

The data in Table 3 show that 1,2- and 1,3-H-atom transfers (with highly strained three- and four-membered rings in the transition states, respectively) have the highest activation energies, at about 170 kJ mol^{-1}. As the transition-state ring structures become larger and conformations are more relaxed, the barriers significantly decrease to about 75−80 kJ mol^{-1} for 1,5- and 1,6-H-atom transfers (six- and seven-membered rings). For even larger transition-state structures, the barriers slightly increase (about 15 kJ mol^{-1}) to about 90 kJ mol^{-1}.

The lowest barrier to reaction occurs for the 1,6-H-atom transfer (∼76 kJ mol^{-1}). This process can be compared with a simple bimolecular abstraction reaction: propane + 1-propyl → 1-propyl + propane (CCC−H + *CCC → CCC* + H−CCC), which has a barrier of about 65 kJ mol^{-1}. Both the unimolecular H-atom isomerizations and the bimolecular H-atom abstractions involve one primary C−H bond breaking and one primary C−H bond forming. The relatively small difference (∼11 kJ mol^{-1}) between the barriers in the formal abstractions and the internal abstractions (in the "unstrained" rings) can be attributed to simple conformational differences that can range from about 5 kJ mol^{-1} for gauche interactions (e.g., staggered conformations) up to 25 kJ mol^{-1} for syn interactions.in alkanes (e.g., eclipsed conformations).

The general trend observed in barrier heights for H-atom transfers follows known trends in ring strains of cycloalkanes. Ring strains are often computed using group additivity: taking the difference between the experimental (or calculated) enthalpy of the formation of the cyclic structure and the sum of enthalpy contributions for each of the groups in the molecule. For example, the enthalpies of formation of cyclohexane and cyclopentane are about −123 and −77 kJ mol^{-1}, respectively.[39] Using a value of −20.5 kJ mol^{-1} for a methylene (−CH$_2$−) group, we compute ring strains of about 0 kJ mol^{-1} for cyclohexane and about 25 kJ mol^{-1} for cyclopentane. This 25 kJ mol^{-1} difference is comparable to the difference in barriers (∼27 kJ mol^{-1}, Table 3) between the 1-butyl → 1-butyl reaction (a five-membered ring) and the 1-pentyl → 1-pentyl reaction (a six-membered ring).

Similar data for H-atom transfer reactions involving the formation of secondary radicals from primary radicals (primary → secondary; e.g., 1-propyl → 2-propyl) are also presented in Table 3 (summary) and the Supporting Information (detailed). For many of these cases, the same product can occur via different pathways: 1-butyl → 2-butyl can occur through both a 1,2-H-atom transfer (CCCC* → CCC*C) and a 1,3-H-atom transfer (CCCC* → CC*CC) because there are two equivalent ends of the molecule. This is also the case with other reactions summarized in Table 3, such as the formation of a secondary radical from a secondary radical.

Figure 5 presents the G3MP2B3 barriers to reaction as a function of the transition-state ring size (a 1,2-H-atom transfer has a three-membered transition state, a 1,3-H-atom transfer has a four-membered transition state, etc.) as well as a curve showing computed ring strain in cycloalkanes. Three- and four-membered transition states have the highest barriers to reaction, roughly 160−170 kJ mol^{-1}. The barriers fall significantly to about 70−80 kJ mol^{-1} for six- and seven-membered transition states (1,5- and 1,6-H-atom transfers) and then increase slightly (by 10 kJ mol^{-1}) for larger structures. Tight structures (small rings) require significant changes in the conformation of the molecule; overall, the correlation between ring strain and transition-state size is reasonable because both depend on the ring size.

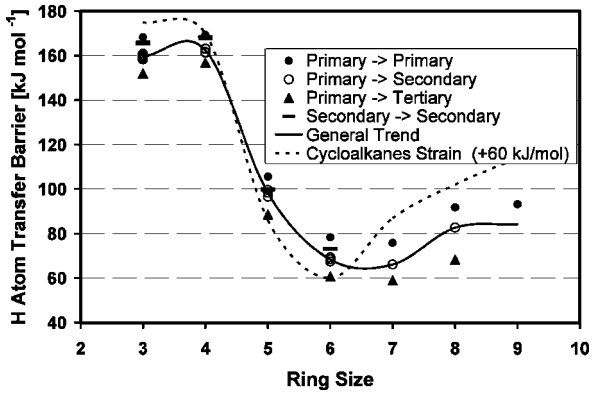

Figure 5. G3MP2B3 barriers to reaction at 0 K for H-atom transfers involving primary, secondary, and tertiary radicals. Ring strains for cycloalkanes are shown for comparison. General uncertainties seen in H-atom transfers were estimated around 6 kJ mol^{-1}, as explained in the Computational Methods section.

Tertiary alkyl radicals are relevant to branched hydrocarbons (e.g., isooctane), which are an important class of molecules in hydrocarbon fuel chemistry. For instance, the β scission of *tert*-butyl radical to yield isobutene and H atom constitutes a crucial reaction step in the combustion of the primary reference fuels.[40,41] In terms of enthalpies of formation and BDEs, tertiary alkyl radicals are about 5 to 6 and 16 to 18 kJ mol^{-1} more stable than secondary and primary alkyl radicals, respectively, and thus may be preferentially formed through isomerizations. Therefore, reaction types involving branched radicals, including primary → tertiary and secondary → tertiary H-atom transfers, have also been considered. Particular attention has been paid to whether the barriers to reaction are influenced by branching at "spectator" sites (not directly involved in reaction) in molecules where steric interactions may be important.

Generic illustrations of H-atom transfer reactions involving tertiary alkyl radicals are given in Figure 3, and barriers for a representative set of 1° → 3° and 2° → 3° radical isomerizations are summarized in Table 3. (The Supporting Information includes more extensive information on computed enthalpies of formation for the transition states along with barriers to isomerizations.) Barriers to reaction for the formation of tertiary radicals from primary radicals (primary → tertiary) are displayed in Figure 5, which shows the barriers to be roughly 10 and 20 kJ mol^{-1} lower than the comparable reactions involving secondary and primary alkyl radicals, respectively (consistent with trends in the stability of the radicals). With respect to transition-state size, the 1,5- and 1,6-H-atom transfers again demonstrate the lowest barriers, about 60 kJ mol^{-1}; these barriers are essentially equivalent to barriers in $R_1-H + {}^*R_2 \rightarrow R_1{}^* + H-R_2$ abstractions.

The effects of substitution were further explored via a preliminary investigation of isomerization barriers in species substituted at spectator sites. Such cases are important in highly branched fuels. For example, consider the two similar reactions (hex-1-yl → hex-5-yl) and (2,2,3,3,4,4-hexamethylhex-1-yl → 2,2,3,3,4,4-hexamethylhex-5-yl). Both reactions are primary → secondary radical isomerizations involving 1,5-H-atom transfers. However, the latter reaction has many methyl substituents; these substituents are not directly participating in the reaction but could influence ring strain (conformational interactions) in the transition state and consequently contribute to the barrier to reaction.

Isomerization barriers were computed for primary → secondary 1,5-H-atom transfers for a series of increasingly methyl-substituted radicals (hex-1-yl through 2,2,3,4-tetramethylhex-1-yl). It was seen that the barrier heights substantially decreased (on the order of 5 kJ mol^{-1}) for each methyl substitution; this was interpreted to mean that the apparent *decrease* in the barrier is due to an *increase* in the energy of the reactant because of steric interactions. As discussed earlier, the barrier to reaction for these isomerizations consists of a nascent barrier to abstraction plus an energy that can be associated with orienting the molecule in a higher-energy conformation (where steric interactions are present). For unbranched, straight-chain alkyl radicals, there are minimal steric interactions in the molecules and additional conformational energies in the transition states. For highly branched alkyl radicals, there are already significant steric interactions in the molecules, and thus there will be minimal additional conformational energies in the transition states. The net result is that an isomerization barrier in a highly branched alkyl radical will be apparently lower than that in a homologous unbranched species because of the smaller energetic contribution from conformational interactions, going from the reactant to the transition state. This dependence of isomerization barriers on the degree of branching in the molecule warrants further investigation, given the importance of branched species in hydrocarbon fuel chemistry.

Alkyl Radical Trends. Table 3 summarizes the barriers to reaction for the H-atom transfers in alkyl radicals with more detailed data given in the Supporting Information. In particular, the 1,4-, 1,5-, and 1,6-H-atom transfers demonstrate a very consistent trend; the barriers to primary → secondary and primary → tertiary H-atom transfers are roughly 9 and 18 kJ mol^{-1} lower than the barriers to primary → primary H-atom transfers, respectively. These changes in the activation enthalpies parallel the relative reaction exothermicities (computed from bond strengths in Table 2 and tables in the Supporting Information) of 11 and 17 kJ mol^{-1}, respectively. In addition, the barriers to secondary → (secondary or tertiary) H-atom transfers are generally 2 kJ mol^{-1} higher than the corresponding barriers to primary → (secondary or tertiary) H-atom transfers. These trends are consistent with an Evans−Polanyi correlation between activation barriers and reaction enthalpies in a homologous series of reactions.[13]

The data presented in Table 3 and Figure 5 suggest that 1,5- and 1,6-H-atom transfers should dominate isomerization pathways and that shorter or longer transfers should play minimal roles because the barriers are significantly higher. This computational result supports direct experimental observation of such product preferences.[2−7] In addition, isomerizations producing tertiary alkyl radicals should occur preferentially to those producing secondary and primary alkyl radicals. However, several other issues must be considered.

First, for reactants with short hydrocarbon chains, the larger transfers are not possible, and thus 1,2- and 1,3-H-atom transfer may contribute.

Second, although the isomerization barriers for these short-range reactions are significantly higher than those for transition states with larger ring structures, the magnitudes of the barriers (about 160−170 kJ mol^{-1}) are not prohibitively large. Consider the C−H BDEs given in Table 2. The BDEs for β-scission reactions (such as 2-propyl → propene + H) are as much as 140 kJ mol^{-1}, or only slightly less (about 20 kJ mol^{-1}) than the isomerization barriers for 1,2- and 1,3-H-atom transfers.

Third, radicals are often produced through abstraction reactions; if the system temperature is sufficiently high enough that abstraction reactions are active pathways, then short-range

H-atom transfers (internal abstractions) could play a kinetic role under some conditions.

Fourth, radicals are often also produced through chemically activated steps[6] such as radical additions (e.g., propene + H → 1-propyl); the energy contained in the newly formed hot molecules can be available for subsequent pathways (e.g., propene + H → [1-propyl]† → 2-propyl). That is, if a hot radical is produced, it has sufficient energy to make even short-range 1,2- and 1,3-H-atom transfer isomerizations feasible, along with longer-range 1,5- and 1,6-H-atom transfers and C−C β scissions (and possibly C−H β scissions).

Fifth, the competition between H-atom transfers and C−C β scissions significantly influences decomposition pathways; this competition is both temperature- and pressure-dependent. At lower temperatures, H-atom transfers control the chemistry because of their lower reaction barriers; at higher temperatures, C−C β scissions control the chemistry because of their higher *A* factors. Dryer and coworkers[15] have utilized this effect, "lumping" radical species in quasi-equilibrium due to facile isomerizations at lower temperatures, to reduce the complexity of detailed chemical kinetic mechanisms. This competition is further complicated by the fact that these reactions are pressure-dependent (especially the β scissions). A consequence of this is that the internal energy distributions are non-Boltzmann; to obtain correct rate expressions, it is necessary to use RRKM/master equation modeling and consider all of the reactions simultaneously. A further discussion of this issue is outside the scope of this article; the interested reader is referred to refs 2−4.

Sixth, chemical functionalities can play a large role in affecting C−H bond strengths. For alkyl radicals, 1,2- and 1,3-H-atom transfers may be of limited importance. However, for radical derivatives of both alkenes and oxofunctionalized species (ketones, aldehydes, esters) where C−H bonds adjacent to the functionality are substantially weaker (30−50 kJ mol^{-1}), shorter H-atom transfers can become important, which is a topic explored in more detail below.

Finally, and of great importance in kinetic terms, although transition states for large H-atom shifts are energetically favored because the cyclic structures are minimally strained, the transition states are entropically disfavored because they are highly constrained relative to the "floppy" molecules. The formation of the cyclic transition state results in the conversion of hindered rotational modes in the "linear" molecule into ring vibrational modes in the cyclic transition state (a loss of one torsional mode for each bond in the ring), which can have a significant impact on the rate of reaction. This entropic consideration directly affects the pre-exponential factor ($A = e^{\Delta S_a/R}$, where ΔS_a refers to the entropy of activation) in the rate constant and can reduce the rate constant by as much as a factor of 3 to 10 per rotor lost.

Alkenyl and Alkanoyl Radicals (Allylic and Oxoallylic). As presented and discussed above, the barriers for H-atom transfers in alkyl radicals heavily depend on both the size of the transfer (e.g., 1,3-H-atom transfer versus 1,5-H-atom transfer) and the type of incipient radical site (e.g., 2° versus 3°). The isomerizations possible for alkenyl and alkanoyl radicals were also explored. These species are important in the combustion of both biodiesel and hydrocarbon fuels: unsaturated fatty esters such as methyl linolenate (9,12,15-octadecatrienoate) or methyl palmitelaidate (9-hexadecenoate) are common components in such fuels, whereas the oxidation of large hydrocarbons generally involves steps in which unsaturated species and aldehydes are formed.

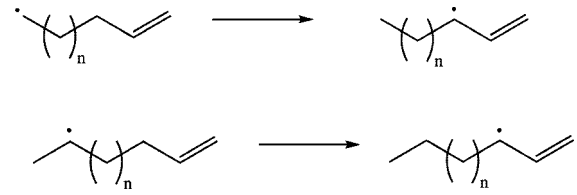

Figure 6. Primary → allylic and secondary → allylic H-Atom transfer isomerizations.

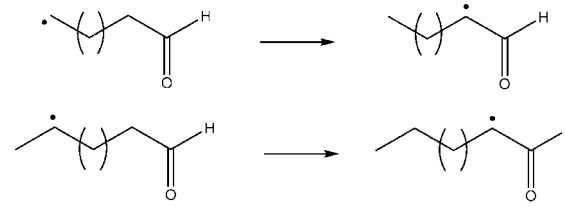

Figure 7. Primary → oxoallylic and secondary → oxoallylic H-atom transfer isomerizations.

Figure 6 illustrates reactions involving H-atom transfers in alkenyl radicals: primary → allylic radical isomerization, where a terminal $-CH_2$* radical group abstracts a H atom from a position immediately adjacent (α) to an alkene bond, and secondary → allylic radical isomerization, where an interior −CH*− radical group is involved in the abstraction.

Figure 7 illustrates the analogous reactions in the case of an aldehyde with a radical center on its side chain. Abstraction of the H-atom in the α position relative to the carbonyl group yields an "oxoallylic" radical. These reactions also occur in ketones. A summary of the computed isomerization barriers for the allylic and oxoallylic radicals is given in Table 4, along with comparisons with those for alkyl radical isomerizations.

More details of many specific cases are given in the Supporting Information, including additional barrier heights and computed enthalpies of formation of relevant radicals and transition states. These data also include H-atom transfer barriers for the comparable reactions in radicals derived from ketones; given their correspondence to the results seen with radicals derived from aldehydes, an exhaustive set of reactions for these species was not calculated. These data show that isomerization barriers involving the analogous ketone-derived radicals are not very different because the 1,2- and 1,3-H-atom transfers in ketone-derived species have barriers of only 2−4 kJ mol^{-1} higher than those in the aldehyde-derived species; in the important 1,5- and 1,6-H-atom transfers, the difference is less than 1 kJ mol^{-1}.

Overall Comparisons. The dependence of reaction barriers on cyclic-transition-state sizes is illustrated in Figure 8 for the case of secondary → secondary radical isomerizations (alkyl, allylic, and oxoallylic). The barriers for the allylic reactions are nearly 20 kJ mol^{-1} lower than the comparable reactions involving saturated alkyl radicals. This difference appears to be only weakly dependent on the size of the transition state; for example, for a 1,2-H-atom migration and a 1,6-H-atom transfer, the respective differences are 23 and 18 kJ mol^{-1}, although these are fundamentally different reactions, as discussed above. However, in the oxoallylic reactions, the barriers are 20−40 kJ mol^{-1} lower than those of the saturated alkyl radicals and 5−20 kJ mol^{-1} lower than those of the allylic radicals. These differences are strongly dependent on the size of the transition state.

These two effects warrant some discussion. First, the C−H bond strength at the α position of an aldehyde (the "oxoallylic" carbon immediately adjacent to the carbonyl group) is roughly

TABLE 4: Summary of G3MP2B3 Barriers for H-Atom Transfers for Radicals of Alkanes, Alkenes, and Aldehydes[a]

	alkyl C−C−C*					allylic C=C−C*		oxoallylic O=C−C*	
transfer	$E_0(1° \rightarrow 1°)$/kJ mol^{-1}	$E_0(2° \rightarrow 2°)$/kJ mol^{-1}	$E_0(1° \rightarrow 2°)$/kJ mol^{-1}	$E_0(2° \rightarrow 3°)$/kJ mol^{-1}	$E_0(1° \rightarrow 3°)$/kJ mol^{-1}	$E_0(1° \rightarrow 2°)$/kJ mol^{-1}	$E_0(2° \rightarrow 2°)$/kJ mol^{-1}	$E_0(1° \rightarrow 2°)$/kJ mol^{-1}	$E_0(2° \rightarrow 2°)$/kJ mol^{-1}
2	168.3	165.5	159.5	163.5	151.9	139.3	142.6	122.3	122.8
3	169.3	167.9	162.4	161.1	156.8	150.1	149.0	135.9	136.1
4	105.6	99.8	98.3	91.0	88.6	84.5	80.2	76.9	73.1
5	78.4	73.1	68.4	62.9	60.7	56.2	54.1	49.7	48.4
6	75.9	67.9	66.1	58.3	58.9	53.9	50.0	48.3	46.8
7	91.8	85.0	82.7	68.2	68.2	66.2	65.4	66.2	66.3
8	93.3		84.2						
$\Delta(E_a)$[b]	+9	+3	0	−7	−8	−13	−16	−19 (−37)	−20 (−37)

[a] See the Supporting Information for data for individual reactions. [b] Average barriers for unstrained structures relative to primary → secondary radical isomerizations (1° → 2°) in alkyl radicals. Values given in parentheses are for 1,2-H-atom migrations when significantly different than the "internal" abstractions.

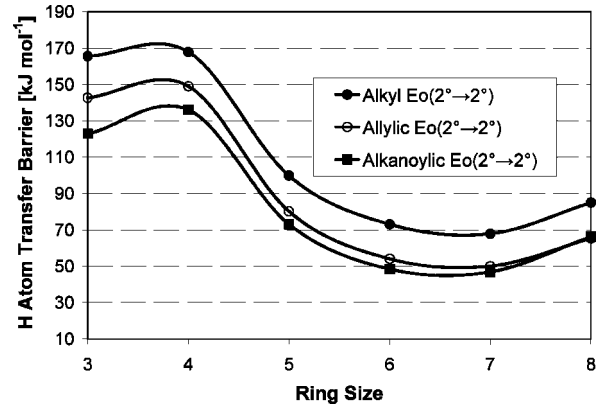

Figure 8. Secondary → secondary alkyl, allylic, and oxoallylic H-atom transfer isomerizations.

373 kJ mol^{-1}; this value is greater than an allylic C−H bond strength by about 20 kJ mol^{-1}. (See Table 2 and the Supporting Information.) Consequently, it might be expected that the barriers for H-atom transfers would also be higher for the oxoallylic cases compared with the allylic cases, as would be consistent with an Evans−Polanyi correlation between activation energies and reaction. In reality, the oxoallylic radicals demonstrate barrier heights that are 5−20 kJ mol^{-1} lower than those of the allylic radicals. Second, the relative barriers for the allylic and oxoallylic radicals are roughly equal for "unstrained" transition states (large transfers), whereas there are large differences of about 15−20 kJ mol^{-1} seen for the small transfers.

Therefore, the barriers for reactions involving allylic radicals are *higher* than and the barriers for oxoallylic radicals are *lower* than what would be expected when considering a simple correlation between activation energies and enthalpies of reactions in a homologous series of reactions, as was seen in the alkyl radicals. This means that the reactions of these functionalized species are *not* homologous with those of alkyl radicals.

These effects can be attributed in part to the electronegativity of the oxygen atom in the carbonyl group. The formation of allylic species, seen in the alkenyl radical reactions, involves significant rehybridization of the α carbon; in the oxoallylic radical reactions, the electron-withdrawing nature of oxygen retards this rehybridization ("weakening" the bond by keeping its sp^3 character and facilitating the abstraction). For the reactions involving allylic radical formation, the transition states look very "product-like" (alkene-like), with the radical carbon site in a near-planar (sp^2) geometry; the nonreacting allylic H atom is roughly 6° out-of-plane for the 1,2-H-atom transfers and around 12° out-of-plane for 1,3-transfers and larger. In contrast, for the oxoallylic radical formation reactions, the radical sites in the transition states are more distinctly nonplanar and look more "reactant-like" (alkane-like, with greater sp^3 character); the nonreacting allylic H atom is about 8° out-of-plane for the 1,2-H-atom transfers and about 26° out-of-plane for 1,3-H-atom (and larger) transfers. These oxoallylic transition states are similar to those of simple alkyl radicals, where the radical sites are about 8 and 31° out-of-plane for 1,2-H-atom and for 1,3-H-atom (and larger) transfers, respectively. These effects are more pronounced in smaller, strained transition states across all reaction classes.

Potential electronegative effects were subjected to a fuller analysis; the concept that the electronegativity of functional groups affects resonance stabilization and rehybridization was explored by computing barriers to isomerization in fluorine-

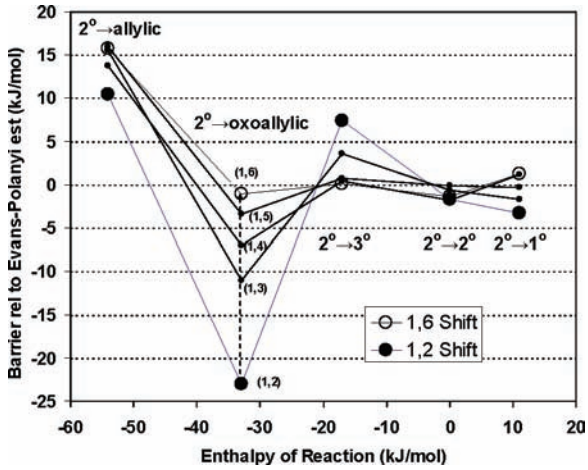

Figure 9. Barrier heights relative to Evans−Polanyi derived predictions for 1,2- through 1,6-H-atom transfers.

substituted analogues. These data are explicitly provided in the Supporting Information; here we simply provide an overview. The computed data show that a fluorine atom can lower barriers in certain cases by stabilizing radicals immediately adjacent (α) to the substitution on the order of 5 kJ mol^{-1}. However, this difference is significantly less than the 20 kJ mol^{-1} difference seen between barriers for allylic and oxoallylic radical isomerizations. Consequently, these results are considered to be somewhat inconclusive and to merit further investigation.

However, direct identification of the degree of hybridization of the radicals via the planarity of the radical site is conclusive. This indicates that the H-atom transfers involving alkyl and oxoallylic radicals proceed with a greater degree of sp^3 hybridization at the radical site than do the reactions involving allylic radicals. Consequently, one might expect that the energetics of allylic radical isomerizations (barrier heights and enthalpies of reaction) should not be correlated with those for simple alkyl radicals. A practical consequence of this is that a broad-brush application of estimation methods using generic Evans−Polanyi correlations is likely to yield significantly erroneous results if the reactions under investigation are not truly homologous, as seen in these cases.

Implications of Non-Evans−Polanyi Behavior. This important conclusion is further explored in Figure 9, which shows the deviations of the computed G3MP2B3 barriers from those estimated using correlation equations such as those given earlier (eqs 1−3). We used generic ring strains of 167, 169, 102, 73, and 69 kJ mol^{-1} for the A coefficient in 1,2- through 1,6-H transfers, respectively, and a coefficient of 0.65 for the change in the barrier with respect to the enthalpy of reaction: $E_a = A + (0.65)\Delta_{rxn}H$. (These parameters were simply "best fit" values that replicated data given in Table 4; we do not consider these values to be applicable to other types of reactions.) The alkyl radicals follow this correlation well, within about 3 kJ mol^{-1}. However, the reactions involving allylic radicals have barriers that are significantly higher (about 15 kJ mol^{-1}) than would be predicted, assuming a simple correlation between barrier heights and enthalpies of reaction; furthermore, those reactions involving oxoallylic radicals are not only significantly lower than would be predicted but are also strongly dependent on the ring size (varying from 1 to almost 25 kJ mol^{-1} lower).

In short, employing Evans−Polanyi type estimation methods appears to work well for simple alkyl radicals but can lead to serious errors in allylic and oxoallylic radicals. These observed trends are consistent with the idea that the degree of hybridization of the radical site involved in the cyclic transition state influences the degree of ring strain. A fully sp^2-hybridized radical center would "flatten out" a portion of the cyclic transition state and cause additional strain, a phenomenon that would be more or less visible given the size of the ring, whereas a fully sp^3-hybridized radical center would invoke minimal ring strain. By analogy, the ring strain for cyclohexene is ∼6 kJ mol^{-1} higher than that for cyclohexane, whereas the ring strain for cyclobutene is ∼15 kJ mol^{-1} higher than that for cyclobutane.

The implications of the trends in barrier heights is illustrated in Figure 9, which shows that transition states involving partially sp^2-hybridized allylic radicals (late, alkenyl-product-like) have higher barriers than those involving sp^3-hybridized alkyl radicals. Conversely, transition states having partially sp^3-hybridized oxoallylic radicals (early, alkyl-reactant-like) have lower barriers than those for alkyl radicals.

The practical consequence of these effects on combustion chemistry modeling is that the use of generic Evans−Polanyi correlations to predict barriers where reactions are not fully homologous can lead to significant errors on the order of as much as 15−20 kJ mol^{-1}. Ours is not the first study to identify this problem. The NIST combustion chemistry measurement program of Tsang and coworkers[3−7] is specifically directed at providing rate expressions for such critical reactions. Other researchers, such as Sarofim and coworkers,[42] have recognized through both experimental measurements and modeling studies that the uncertainties in rate expressions for isomerization and β-scission reactions are major sources of inconsistencies between different combustion chemistry mechanisms and are responsible for differences observed between modeling predictions and experimental measurements.

Conclusions

In summary, we studied the H-atom transfers possible for several alkyl, alkenyl, and oxoallylic radicals in detail, paying particular attention to the potential Evans−Polanyi correlations between the thermodynamics and kinetics of these reactions. Enthalpies of activation were seen to roughly scale with enthalpies of reaction for alkyl radicals but not for the allylic and oxoallylic radicals. This lack of correlation has serious implications in widely utilized[14−19] Evans−Polanyi-like methods for estimating barrier heights used in rate expressions that are subsequently employed in combustion chemistry mechanisms.

Barriers to internal H-atom transfers were seen to correlate generally well with the ring strain present in the transition state. In relatively unstrained systems, the barriers to H-atom transfer were comparable to those for simple H-atom abstractions; the difference between the two types of reaction barriers is about 10 kJ mol^{-1}, which is equivalent to the energetic cost of a gauche repulsion in a hydrocarbon chain. Increased alkyl substitution stabilized incipient radicals by a substantial amount: secondary radicals were formed roughly 10 kJ mol^{-1} more readily than primary radicals, and tertiary radicals were formed roughly 20 kJ mol^{-1} more readily than primary radicals.

Barriers to isomerization were significantly influenced by the presence of adjacent chemical functionalities such as double bonds or carbonyl groups. Barriers for reactions forming allylic radicals were higher than those for reactions forming oxoallylic species; this was attributed to a rehybridization of the reaction center in the allylic cases (product-like transition states and higher barriers). This rehybridization was retarded in the oxoallylic cases because of effects from the electron-withdrawing carbonyl group (leading to reactant-like transition states and lower barriers).

This work suggests the need for a greater reliance on experimental data and ab initio methods for predicting barrier heights and less reliance on generic estimation schemes. The G3MP2B3 method is capable of replicating these known trends to an impressive degree, making it a logical approach for further studying radical reactions with implications in hydrocarbon and biodiesel combustion. Future work will utilize the data presented here to develop rate expressions for use in combustion modeling applications.

Supporting Information Available: More expansive set of enthalpies of formation, barriers to reaction, primary → primary transfers, data for H-atom transfer reactions involving the formation of secondary radicals from primary radicals, and data from computing barriers to isomerization in fluorine-substituted analogues. This material is available free of charge via the Internet at http://pubs.acs.org.

References and Notes

(1) NIST Real Fuels Project Home Page. http://kinetics.nist.gov/realfuels/.

(2) McGiven, W. S.; Awan, I. A.; Tsang, W.; Manion, J. A. Isomerization and decomposition reactions in the pyrolysis of branched hydrocarbons: 4-methyl-1-pentyl radical. *J. Phys. Chem. A* **2008**, *112*, 6908–6917.

(3) Tsang, W.; Walker, J. A.; Manion, J. A. The decomposition of normal hexyl radicals. *Proc. Combust. Inst.* **2007**, *31*, 141–148.

(4) McGivern, W. S.; Manion, J. A.; Tsang, W. Ring-expansion reactions in the thermal decomposition of *tert*-butyl-1,3-cyclopentadiene. *J. Phys. Chem. A* **2006**, *110*, 12822–12831.

(5) Tsang, W. Ring-expansion reactions in the thermal decomposition of *tert*-butyl-1,3-cyclopentadiene. *J. Phys. Chem. A* **2006**, *110*, 8501–8509.

(6) Tsang, W.; Bedanov, V.; Zachariah, M. R. Unimolecular decomposition of large organic radicals with low reaction thresholds: Decomposition and reversible isomerization of *n*-pentyl radical. *Ber. Bunsen−Ges.* **1997**, *101*, 491–499.

(7) Tsang, W.; Walker, J. A. Pyrolysis of 1,7-octadiene and the kinetic and thermodynamic stability of allyl and 4-pentenyl radicals. *J. Phys. Chem.* **1992**, *96*, 8378–8384.

(8) NIST Chemical Kinetics Database, NIST Standard Reference Database Number 17; Allison, T. C., Manion, J. A., Eds.; http://kinetics.nist.gov/ (accessed Aug 2008).

(9) NIST Chemical Kinetics Model Database, Burgess, D. R., Jr., Manion, J. A., Eds.; http://kinetics.nist.gov/CKMech (accessed Aug 2008).

(10) NIST Chemistry WebBook, NIST Standard Reference Database Number 69; Linstrom, P. J., Mallard, W. G., Eds.; http://webbook.nist.gov/ (accessed Aug 2008).

(11) NIST Computational Chemistry Comparison and Benchmark Database, NIST Standard Reference Database Number 101; Johnson, R. D., III., Ed.; http://cccbdb.nist.gov/ (accessed Aug 2008).

(12) Benson, S. W. *Thermochemical Kinetics*; Wiley: New York, 1968.

(13) Evans, M. G.; Polanyi, M. Inertia and driving force of chemical reactions. *Trans. Faraday Soc.* **1938**, *34*, 11–23.

(14) Battin-Leclerc, F. Detailed chemical kinetic models for the low-temperature combustion of hydrocarbons with application to gasoline and diesel fuel surrogates. *Prog. Energy Combust. Sci.* **2008**, *34*, 440–498.

(15) Chaos, M.; Kazakov, A.; Zhao, Z. W.; Dryer, F. L. A high-temperature chemical kinetic model for primary reference fuels. *Int. J. Chem. Kinet.* **2007**, *39*, 399–414.

(16) Yahyaoui, M.; Djebaili-Chaumeix, N.; Dagaut, P.; Paillard, C. E.; Gail, S. Experimental and modelling study of gasoline surrogate mixtures oxidation in jet stirred reactor and shock tube. *Proc. Combust. Inst.* **2007**, *31*, 385–391.

(17) Curran, H. J.; Gaffuri, P.; Pitz, W. J.; Westbrook, C. K. A comprehensive modeling study of *n*-heptane oxidation. *Combust. Flame* **1998**, *114*, 149–177.

(18) Matheu, D. M.; Green, W. H.; Grenda, J. M. Capturing pressure-dependence in automated mechanism generation: Reactions through cycloalkyl intermediates. *Int. J. Chem. Kinet.* **2003**, *35*, 95–119.

(19) Grenda, J. M.; Bozzelli, J. W. *GAPP*, version 1.0; ExxonMobil Research and Engineering Company: Annandale, NJ, 2000.

(20) Hayes, C. J.; Burgess, D. R., Jr. Exploring the oxidative decomposition of methyl esters: methyl butanoate and methyl pentanoate as model compounds for biodiesel. *Proc. Combust. Inst.* **2009**, *32*, 263–270.

(21) Robertson, S. H.; Pilling, M. J.; Jitariu, L. C.; Hillier, I. H. Master equation methods for multiple well systems: application to the 1-, 2-pentyl system. *Phys. Chem. Chem. Phys.* **2007**, *9*, 4085–4097.

(22) Knepp, A. M.; Meloni, G.; Jusinski, L. E.; Taatjes, C. A.; Cavfallotti, C.; Klippenstein, S. J. Theory, measurements, and modeling of OH and HO2 formation in the reaction of cyclohexyl radicals with O_2. *Phys. Chem. Chem. Phys.* **2007**, *9*, 4215–4331.

(23) Ogura, T.; Miyoshi, A.; Koshi, M. Rate coefficients of H-atom abstraction from ethers and isomerization of alkoxyalkylperoxy radicals. *Phys. Chem. Chem. Phys.* **2007**, *9*, 5133–5142.

(24) Merle, J. K.; Hayes, C. J.; Zalyubovsky, S. J.; Glover, B. G.; Miller, T. A.; Hadad, C. M. Theoretical determinations of the ambient conformational distribution and unimolecular decomposition of *n*-propylperoxy radical. *J. Phys. Chem. A* **2005**, *109*, 3637–3646.

(25) DeSain, J. D.; Taatjes, C. A.; Miller, J. A.; Klippenstein, S. J.; Hahn, D. K. Infrared frequency-modulation probing of product formation in alkyl plus O_2 reactions. Part IV. Reactions of propyl and butyl radicals with O_2. *Faraday Discuss.* **2001**, *119*, 101–120.

(26) Chan, C. J.; Hamilton, I. P.; Pritchard, H. O. Self-abstraction in aliphatic hydroperoxyl radicals. *Faraday Trans.* **1998**, *94*, 2303–2306.

(27) Herbinet, O.; Pitz, W. J.; Westbrook, C. K. Detailed chemical kinetic oxidation mechanism for a biodiesel surrogate. *Combust. Flame* **2008**, *154*, 507–528.

(28) Huynh, L. K.; Violi, A. Thermal decomposition of methyl butanoate: ab initio study of a biodiesel fuel surrogate. *J. Org. Chem.* **2008**, *73*, 94–101.

(29) El-Nahas, A. M.; Navarro, M. V.; Simmie, J. M.; Bozzelli, J. W.; Curran, H. J.; Dooley, S.; Metcalfe, W. Enthalpies of formation, bond dissociation energies, and reaction paths for the decomposition of model biofuels: ethyl propanoate and methyl butanoate. *J. Phys. Chem. A* **2007**, *111*, 3727–3739.

(30) Curtiss, L. A.; Raghavachari, K.; Redfern, P. C.; Pople, J. A. Assessment of Gaussian-3 and density functional theories for a larger experimental test set. *J. Chem. Phys.* **2000**, *112*, 7374–7383.

(31) Curtiss, L. A.; Redfern, R. C.; Raghavachari, K.; Pople, J. A. Gaussian-3X (G3X) theory: use of improved geometries, zero-point energies, and Hartree−Fock basis sets. *J. Chem. Phys.* **2001**, *114*, 108–117.

(32) Becke, A. D. Density-functional thermochemistry. 3. The role of exact exchange. *J. Chem. Phys.* **1993**, *98*, 5648–5652.

(33) Lee, C.; Yang, W.; Parr, R. G. Development of the Colle−Salvetti correlation energy formula inta a functional of the electron density. *Phys. Rev. B* **1988**, *37*, 785–789.

(34) Montgomery, J. A.; Frisch, M. J.; Ochterski, J. W.; Petersson, G. A. A complete basis set model chemistry. VI. Use of density functional geometries and frequencies. *J. Chem. Phys.* **1999**, *110*, 2822–2827.

(35) Lynch, B. J.; Fast, P. L.; Harris, M.; Truhlar, D. G. Adiabatic connection for kinetics. *J. Phys. Chem. A* **2000**, *104*, 4811–4815.

(36) Frisch, M. J.; Trucks, G. W.; Schlegel, H. B.; Scuseria, G. E.; Robb, M. A.; Cheeseman, J. R.; Montgomery, J. A., Jr.; Vreven, T.; Kudin, K. N.; Burant, J. C.; Millam, J. M.; Iyengar, S. S.; Tomasi, J.; Barone, V.; Mennucci, B.; Cossi, M.; Scalmani, G.; Rega, N.; Petersson, G. A.; Nakatsuji, H.; Hada, M.; Ehara, M.; Toyota, K.; Fukuda, R.; Hasegawa, J.; Ishida, M.; Nakajima, T.; Honda, Y.; Kitao, O.; Nakai, H.; Klene, M.; Li, X.; Knox, J. E.; Hratchian, H. P.; Cross, J. B.; Bakken, V.; Adamo, C.; Jaramillo, J.; Gomperts, R.; Stratmann, R. E.; Yazyev, O.; Austin, A. J.; Cammi, R.; Pomelli, C.; Ochterski, J. W.; Ayala, P. Y.; Morokuma, K.; Voth, G. A.; Salvador, P.; Dannenberg, J. J.; Zakrzewski, V. G.; Dapprich, S.; Daniels, A. D.; Strain, M. C.; Farkas, O.; Malick, D. K.; Rabuck, A. D.; Raghavachari, K.; Foresman, J. B.; Ortiz, J. V.; Cui, Q.; Baboul, A. G.; Clifford, S.; Cioslowski, J.; Stefanov, B. B.; Liu, G.; Liashenko, A.; Piskorz, P.; Komaromi, I.; Martin, R. L.; Fox, D. J.; Keith, T.; Al-Laham, M. A.; Peng, C. Y.; Nanayakkara, A.; Challacombe, M.; Gill, P. M. W.; Johnson, B.; Chen, W.; Wong, M. W.; Gonzalez, C.; Pople, J. A. Gaussian 03, revision D.01; Gaussian, Inc.: Wallingford, CT, 2004.

(37) Certain commercial equipment, instruments, or materials are identified to specify the procedures adequately. Such identification is not intended to imply recommendation or endorsement by the National Institute of Standards and Technology, nor is it intended to imply that the materials or equipment identified are necessarily the best available for the purpose.

(38) Wijaya, C. D.; Sumathi, R.; Green, W. H. Thermodynamic properties and kinetic parameters for cyclic ether formation from hydroperoxyalkyl radicals. *J. Phys Chem. A* **2003**, *107*, 4908–4920.

(39) Prosen, E. J.; Johnson, W. H.; Rossini, F. D. Heats of formation and combustion of the normal alkylcyclopentanes and cyclohexanes and the increment per CH_2 group for several homologous series of hydrocarbons. *J. Res. Nat. Bur. Stand.* **1946**, *37*, 51–56.

(40) El Kadi, B.; Baronnet, F. Study of the oxidation of unsymmetrical ethers (ETBE, TAME) and tentative interpretation of their high octane numbers. *J. Chim. Phys.* **1995**, *92*, 706–725.

(41) Brocard, J. C.; Baronnet, F.; O'Neal, H. E. Chemical kinetics of the oxidation of methyl tert-butyl ether (MTBE). *Combust. Flame* **1983**, *52*, 25–35.

(42) Zhang, H. Z. R.; Eddings, E. G.; Sarofim, A. F. Olefin chemistry in a premixed n-heptane flame. *Energy Fuels* **2007**, *21*, 677–685.

JP810147Z